




Article

Chemically Bound Resorbable Ceramics as an Antibiotic Delivery System in the Treatment of Purulent–Septic Inflammation of Bone Tissue

Yuliya Lukina ^{1,2,*}, Yuriy Panov ³, Ludmila Panova ⁴, Aleksandr Senyagin ⁵, Leonid Bionyshev-Abramov ¹, Natalya Serejnikova ^{1,6}, Aleksey Kireynov ⁷, Sergey Sivkov ⁸, Nikolay Gavryushenko ¹, Dmitriy Smolentsev ¹, Otabek Toshev ⁹, Dmitriy Lemenovsky ⁴ and Dmitriy Krutko ⁴

- ¹ National Medical Research Center for Traumatology and Orthopedics named after N.N. Priorov, Ministry of Health of the Russian Federation, Priorova 10, 127299 Moscow, Russia; sity-x@bk.ru (L.B.-A.); natalia.serj@yandex.ru (N.S.); gavryushenkons@cito-priorov.ru (N.G.); smolentsev@cito-priorov.ru (D.S.)
- ² Faculty of Digital Technologies and Chemical Engineering, Mendeleev University of Chemical Technology of Russia, Miusskaya pl. 9, 125047 Moscow, Russia
- ³ Bioanalytical Laboratory, Institute of Clinical Research and Pharmaceutical Expertise, Ugreshskaya, 2(8), 115088 Moscow, Russia; jurjypanov@rambler.ru
- ⁴ Department of Chemistry, Lomonosov Moscow State University, Leninskie Gory, 1, b.3, 119991 Moscow, Russia; ludaerkh@gmail.com (L.P.); dali@org.chem.msu.ru (D.L.); kdp@org.chem.msu.ru (D.K.)
- ⁵ Department of Medicine, Peoples Friendship University of Russia (RUDN University), Miklukho-Maklaya 6, 117198 Moscow, Russia; senyaagin_an@pfur.ru
- ⁶ Institute for Regenerative Medicine, Sechenov First Moscow State Medical University, Trubetskaya, 8, 119991 Moscow, Russia
- ⁷ Department of Material Processing Technologies, Bauman Moscow State Technical University, 2 Baumanskaya, 5, b.1, 105005 Moscow, Russia; aleksey.kireynov@emtc.ru
- ⁸ Faculty of Technology of Inorganic Substances and High-Temperature Materials, Mendeleev University of Chemical Technology of Russia, Miusskaya pl. 9, 125047 Moscow, Russia; sikov.s.p@muctr.ru
- ⁹ Department of Materials Science, Lomonosov Moscow State University, Leninskie Gory, 1, 119991 Moscow, Russia; otabetoshev0995@mail.ru
- * Correspondence: lukina_rctu@mail.ru



Citation: Lukina, Y.; Panov, Y.; Panova, L.; Senyagin, A.; Bionyshev-Abramov, L.; Serejnikova, N.; Kireynov, A.; Sivkov, S.; Gavryushenko, N.; Smolentsev, D.; et al. Chemically Bound Resorbable Ceramics as an Antibiotic Delivery System in the Treatment of Purulent–Septic Inflammation of Bone Tissue. *Ceramics* **2022**, *5*, 330–350. <https://doi.org/10.3390/ceramics5030026>

Academic Editor: Francesco Baino

Received: 30 June 2022

Accepted: 22 July 2022

Published: 27 July 2022

Publisher's Note: MDPI stays neutral with regard to jurisdictional claims in published maps and institutional affiliations.



Copyright: © 2022 by the authors. Licensee MDPI, Basel, Switzerland. This article is an open access article distributed under the terms and conditions of the Creative Commons Attribution (CC BY) license (<https://creativecommons.org/licenses/by/4.0/>).

Abstract: Local drug delivery systems are an effective approach in the treatment of purulent–septic inflammation of bone tissue. Chemically bonded multiphase ceramics based on calcium-deficient carbonate-substituted hydroxyapatite combine resorbability, osteoconductivity, and the possibility of volumetric incorporation of antibiotics. Macroporosity is regulated by the concentration of polyethylene glycol granules introduced into the initial powder composition, followed by their extraction. The selected conditions for the consolidation of the ceramic matrix and the extraction of PEG granules retain the activity of vancomycin, which is confirmed by the results of microbiological studies. The concentration of vancomycin and the porosity affect the local concentration and release of the antibiotic. The incorporation method provides a prolonged release of the antibiotic for up to 31 days. In vivo experiments with bone implantation have shown that chemically bound macroporous ceramics with incorporated vancomycin are a therapeutically effective carrier of the substance during the healing of bone defects in conditions of surrounding purulent–septic inflammation, and can be considered as a carrier for local antibacterial therapy, at the site of implantation.

Keywords: prolonged release; antibiotic; consolidation; carbonate-substituted hydroxyapatite; macroporosity; PEG; resorbability; vancomycin; purulent–septic inflammation

1. Introduction

Osteomyelitis is a serious problem in bone surgery, whose treatment traditionally includes rehabilitation of necrotic and infected areas of bone and soft tissues, along with long-term systemic administration of antibiotics, filling in the formed defect [1,2].

The most common causative agent of bone infection, which causes approximately 75% of cases of osteomyelitis, is conditionally pathogenic Gram-positive *Staphylococcus aureus* [3,4]. Other pathogens include enterococci, streptococci, *Pseudomonas aeruginosa*, and enterobacteria [5].

Vancomycin is the most common and effective broad-spectrum antibiotic for parenteral administration; it is a glycopeptide active against Gram-positive bacteria. In polymicrobial infections, combinations of glycopeptide and gentamicin or glycopeptide and anti-pseudomonad are used [6].

Systemic use of antibiotics requires a large dose to obtain locally acceptable concentrations, due to the limited antibiotic delivery to infected wounds. This concentration is often insufficient to kill bacteria [7], and can cause side effects and prolonged recovery [8]. Local infection can develop into chronic osteomyelitis and persist for months or years, which leads to a long hospital stay for patients [9], and possible limb necrosis, dysfunction, and sepsis [10]. For example, approximately 20% of diabetic foot ulcers—which occur in 25% of diabetic patients—will spread to nearby bone tissues and result in osteomyelitis [11].

In addition to the accepted systemic approaches to the treatment of osteomyelitis after surgical wound treatment, local drug delivery systems have been a more effective approach in recent decades [8,12].

Local drug delivery systems using carriers have advantages in increasing the possibility of penetration of antimicrobial agents into bone tissues, ensuring prolonged release and localized concentrations of antimicrobial agents in the infused zone, while avoiding systemic side effects and toxicity [13]. The use of optimal carriers, the necessary concentrations of antimicrobials, and control of the release rate of the drug can help in the fight against infection and limit the frequency of relapses [12].

As antibiotic delivery systems, the most studied materials are bioresorbable materials, including calcium sulfate, demineralized bone matrix, calcium phosphate, bioglass, collagen, gelatin, chitosan, polylactide, and polyglycolide, in various forms of delivery [14–17], some of which are commercial products [14].

Matrices based on chemically bonded calcium phosphate ceramics are a promising type of scaffold for the treatment of osteomyelitis, due to their similarity in composition with the mineral component of bone tissue, high specific surface area, and increased resorption rate compared with matrices obtained via high-temperature treatment. The frameworks are formed due to the interaction of the compressed initial components in the aqueous medium due to setting and hardening, and are an excellent platform for the incorporation of antibacterial agents at the mixing stage, with the possibility of changing the release kinetics and stimulation of osteogenesis.

According to data from the literature, the activity of the antibiotic does not decrease when it is mixed into calcium phosphate cements of various compositions, and does not affect the phase composition and properties of the cement stone, remaining as a separate solid phase during setting, and spreading along the pores of the cement stone [18–20]. The release of the antibiotic during incorporation is smoother than during impregnation, and depends on the composition and porosity of the calcium phosphate cement [21].

The interconnected open microporous system provides good impregnation of the material with biological fluids, oxygen diffusion, and surface roughness, which plays an important role in the adsorption and retention of osteogenic cells on the implant surface. Macropores (over 100 microns in size) facilitate cell infiltration and migration into the scaffold, along with angiogenesis [22–24].

The most popular method of forming macroporosity is the method of removing introduced pore-forming additives, which include crystals, particles, or fibers of burnt or soluble substances, e.g., paraffin, or soluble salts of alkali metals, provided in direct form or in the form of compounds containing certain anions and cations that form alkali metal salts—for example, potassium chloride, sodium, calcium, sodium citrate, sodium or potassium hydroxide, sodium bicarbonate and phosphate salts [25–28].

Removal of the threshold by burning or washing out water-soluble salts in an aqueous medium is unacceptable for chemically bonded ceramics with incorporated antibacterial agents, since it will lead to volatilization or removal of the antibiotic. Therefore, the only solution to create macroporous chemically crosslinked ceramics is to wash out the porogen with organic solvents in which the antibiotic does not dissolve.

The purpose of this work is to create resorbable microporous chemically bonded ceramics based on carbonate-substituted calcium-deficient hydroxyapatite containing antibacterial substances for the treatment of purulent–septic inflammation of bone tissue. As far as we know, this is the first study that describes a low-temperature technology for producing a bioresorbable calcium phosphate matrix with macroporosity and volumetric filling with an antibiotic. The clinical effectiveness of the developed ceramics is determined to a greater extent by the prolonged release of the drug and the ability of the material to be replaced by newly formed bone tissue. Gradual resorption of the material can lead to the secondary release of the antibiotic, increasing the antimicrobial efficacy at the stage of bone tissue restoration. An important feature of the developed material is volumetric incorporation, which provides a prolongation of the antibiotic yield compared to surface impregnation, in which a rapid complete initial release is observed [19]. Volumetric incorporation is possible only with the use of low-temperature technologies that preserve its activity.

2. Materials and Methods

Preparation of chemically bonded ceramics.

Into a homogenized mixture of the composition 80% α -Ca₃(PO₄)₂, 8% CaCO₃, 6% Ca(H₂PO₄)₂·H₂O, and 6% Na₂HPO₄·12H₂O, various amounts of polyethylene glycol granules (hereafter referred to as PEG) were added by weight, with a size of 100–600 microns above the mass of the cement mixture. The mixture moistened with distilled water was subjected to uniaxial pressing at a pressure of 130 MPa, dried in air for a day, and consolidation was carried out in distilled water for 3–72 h at 20–60 °C, after which it was dried in air.

Macroporosity was formed by extraction of PEG from pressed matrices using a Soxhlet apparatus. Chloroform was used as a solvent for PEG extraction. Extraction was implemented for a constant mass of samples, after which drying was implemented in vacuum for 24 h.

The removal of organic solvents from the matrix structure was implemented in a flow reactor in a supercritical fluid CO₂ environment with stirring at a temperature of 70 °C and a pressure of 10 MPa for 6 h.

The mechanical strength of the matrices was determined on samples of 10 mm × 10 mm × 30 mm by means of an LFM-50 universal testing machine (Walter + Bai AG), at a loading speed of 8 mm/min, on the 7th day after molding.

Incorporation of vancomycin was carried out by adding 150–300 mg of pharmaceutical-grade powder per 3 cm³ matrix to the dry mixture before moistening and pressing it out.

The dynamics of the vancomycin yield were determined by high-performance liquid chromatography on a Thermo Ultimate 3000RS chromatograph (Agilent Poroshell 120 El-C18 column, 3.0 mm × 50 mm 2.7 micron). The sample was placed in a flask equipped with a magnetic stirrer, and 100 mL of distilled water was added. After 0.25, 0.5, 0.75, 1, 1.5, 2, 3, 5, 7, 24, 51, and 75 h, a 500 µL aliquot was taken, which then was analyzed by HPLC UV, and 500 µL of distilled water was added.

The porosity was determined by hydrostatic weighing in an inert liquid.

X-ray powder diffraction (XRD) analysis was performed using an ARL Equinox 1000 X-ray diffractometer (Thermo Fisher Scientific INEL SAS, Waltham, MA, USA). The survey was carried out in the reflection mode using Cu K α radiation (angle interval 2 Θ : from 5° to 50°; step 2 Θ 0.03°). The exposure time was 5 s/per step. In qualitative analysis of the resultant X-ray diffraction patterns, we used WinXPOW software and the ICDD PDF-2 database.

In quantitative analysis, we used the reference intensity ratio method (with the I/I_c intensity ratio of the strongest lines of the substance and corundum ($\alpha\text{-Al}_2\text{O}_3$) in a mixture containing 50 wt.% of both components). The weight fraction was calculated using the following relation:

$$\omega_A = \frac{I_{iA}/(I/I_c(A)) \cdot I_{iA}^{rel}}{\sum I_{iK}/(I/I_c(K)) \cdot I_{iK}^{rel}}$$

where I_{iA} is the measured intensity of the i th reflection from phase A; I_{iA}^{rel} is the relative intensity of this reflection in the database; $I/I_c(A)$ is the corundum number for the phase A being determined; and I_{iK} , I_{iK}^{rel} , and $I/I_c(K)$ are the corresponding quantities for all components of the mixture (including A).

Elemental analysis was carried out by means of a special detector (energy dispersion spectrometer); processing was carried out in the INCA—Point&ID program.

FTIR spectra were captured using the PerkinElmer Spectrum One IR Fourier spectrometer in the transmission mode in the range of 4000–400 cm^{-1} , with a resolution of 1 cm^{-1} (5 mg/50 mg of KBr powder).

The microstructure was studied using a Phenom XL G2 scanning electron microscope (Thermo Fisher Scientific) at an accelerating voltage of 15 kV. Silver was sprayed with a Cressington 108auto magnetron sprayer (Cressington Scientific Instruments Ltd., Watford, UK).

Micro-CT of the samples was performed on a Bruker SkyScan 1172 X-ray microtomograph (Kontich, Belgium) with a rotation step of 0.4 degrees and a resolution of 9 microns, using SkyScan software. As a result of scanning, a set of shadow projections of samples was obtained. Based on the obtained shadow projections, reconstruction was performed in the NRecon program using the Feldkamp algorithm. The necessary cross-sections, reconstruction parameters, and dynamic range were selected to achieve optimal image contrast. Images of volumetric models of samples were obtained using the CTvox program included in the tomography software package. To construct three-dimensional models, the marching cubes algorithm was used, which is an algorithm for constructing a surface based on the model of explicit assignment of hexagonal voxels developed by Lorensen and Klein (1987).

The completeness of PEG removal was controlled by ^1H NMR, using phenanthrene as an internal standard (^1H NMR spectra were recorded on the Bruker Advance-400 spectrometer (operating frequency 400 MHz) in CDCl_3). Samples for NMR were prepared by 4-fold extraction of the crushed matrix in 3 mL of methylene chloride in an ultrasound bath without heating for 10 min, followed by centrifugation and evaporation of the extract in vacuum. The residue was dissolved in 0.6 mL of CDCl_3 .

The determination of antibacterial activity was carried out by measuring the diameter of the growth retardation zones of bacterial cultures—museum reference strains: *St. aureus* ATCC 6538 (Gr+) and *E. coli* ATCC 2582 (Gr−). A sterile saline solution of sodium chloride with a concentration of 0.9% was selected as a negative control (K_1); a sterile saline solution of sodium chloride with a concentration of 0.9% after 24 h of incubation with a test sample without vancomycin at 37 °C was selected as a second negative control (K_2), incubated under the same conditions as the experimental samples; and a test disk was selected as a positive control (K+), with ceftazidime and clavulanic acid (CAC30/10—ceftazidime 30 μg /clavulanic acid 10 mcg; HIMEDIA[®]). Bacterial suspensions were obtained by culturing 100 mL of broth culture in 10 mL of cardio-cerebral broth (HIMEDIA[®] M210) and seeded by the “lawn” method on Muller–Hinton agar (HIMEDIA[®] M211). After sowing, wells with a diameter of 5 mm and a volume of 15 μL were made in agar with a sterile metal punch, after which they were filled with solutions of negative control and a solution obtained after incubation of the matrix for 24 h at a temperature of 37 °C.

Preclinical assessment of the biocompatibility, resorption, and antibacterial effect of the obtained calcium phosphate matrices was carried out in “in vivo” studies on Wistar rats using a model of bone perforation of critical size (2/3 diameter) of the tibia with preformed purulent–septic inflammation. The study was conducted on three animals.

The evaluation of the antibacterial effect was carried out using histological examination, while the evaluation of resorption was carried out by tomographic examination, with the determination of the implant volume by orthogonal projections of the zone of interest using the FEI Avizo 9.0.1 program.

Tomographic examination was carried out in vivo after surgery, and posthumously after 3 months of implantation. Microcomputed tomography (Micro-CT) was performed with a Bruker SkyScan 1178 scanner (Kontich, Belgium), at a voltage of 65 kV and a current of 615 μ A, with a 0.5 mm Al filter. Spatial resolution was 84 microns/pixel. Sections were reconstructed using NRecon v1.6.10.4 software. 3D reconstructions were made in the CT Vol 2.2.0.0 program.

For *histological examination*, samples were fixed in neutral-buffered 10% formalin, decalcified in a special acid solution (SoftyDek, Biovitrum, Stockholm, Sweden), subjected to standard alcohol wiring, and embedded into paraffin blocks. Then, 4 μ m thick paraffin sections were stained with hematoxylin and eosin and picosirius red according to the standard protocols. The obtained microscopic slides were examined with a universal LEICA DM4000 B LED microscope equipped with a LEICA DFC7000 T digital video camera (Leica Microsystems, Wetzlar, Germany) by standard light, phase-contrast, dark-field, and polarized microscopy methods.

3. Results

3.1. Temperature and Time of Consolidation of Ceramics

Acid–base interaction and hydrolysis are the main processes in the formation of chemically bonded ceramics during the interaction of a powder mixture with water.

The influence of technological parameters on the reaction rate, the consolidation temperature, and the particle size of the initial components was investigated in this work.

The solubility of α -tricalcium phosphate (α -TCP) limits the reaction rate, since it has a low solubility of 0.002 g/100 mL. According to X-ray diffraction measurements, the completeness of the reaction at the time depends on the temperature and granulometric composition. Figure 1 shows diffractograms of ceramics consolidated in humid-air conditions for 24 h at a temperature of 20–80 °C, based on α -TCP with the parameters presented in Table 1.

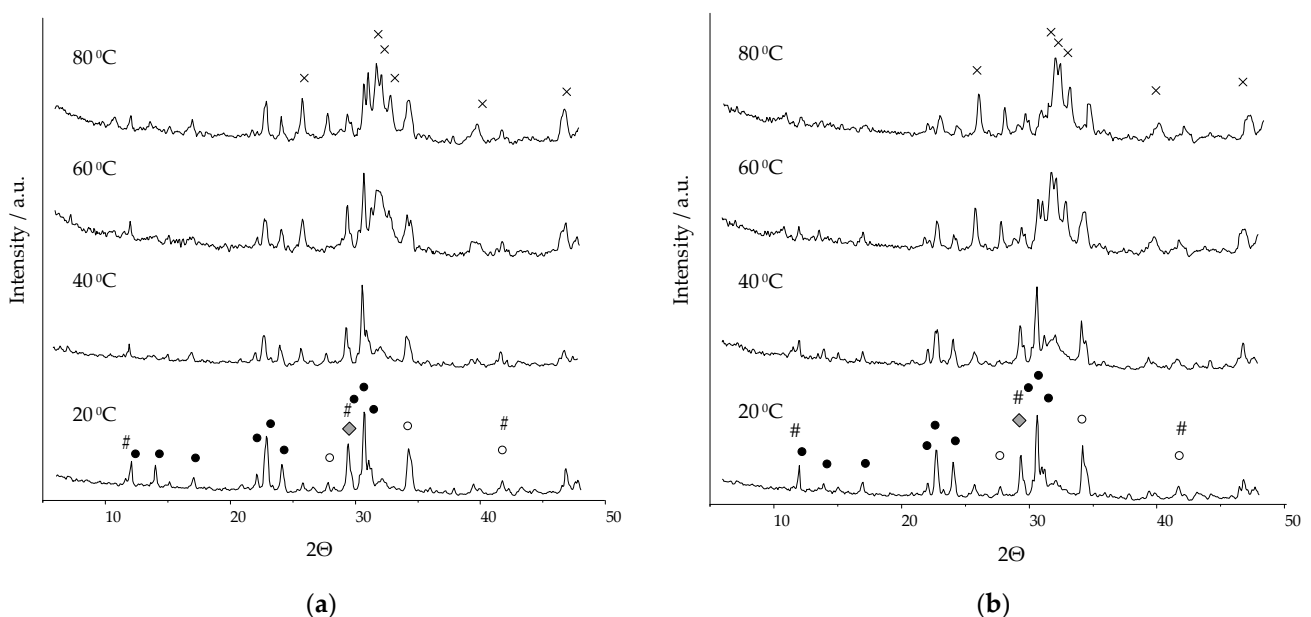


Figure 1. Diffractograms of ceramics consolidated within 24 h based on α -TCP with an average particle size of (a) D [3,4] 37.02 μ m (α -TCP1) or (b) D [3,4] 6.12 μ m (α -TCP2). ●: α -TCP; ○: β -TCP; ◆: CaCO_3 ; X: CO_3 -HAP/dHAP; #: DCPD.

Table 1. Surface area and average particle size of α -TCP under different grinding modes.

Parameter	α -TCP1	α -TCP2
Surface area, m ² /g	1.1080	3.1503
Average particle size D [3,4], μ m	37.02	6.12

The chemically bonded ceramic in the α -Ca₃(PO₄)₂/CaCO₃/Ca(H₂PO₄)₂·H₂O/Na₂HPO₄·12H₂O system with a ratio of the initial components (wt.%) of 80/8/6/6 was a non-stoichiometric carbonate-substituted hydroxyapatite of a composition similar to that of the main mineral component of bone tissue—Ca_{10-x-y/2}(HPO₄)_x(CO₃)_y(PO₄)_{6-x-y}(OH)_{2-x}. X-rays of ceramics formed during hydrolysis and acid–base interaction of the system components showed the presence of carbonate-substituted hydroxyapatite Ca₁₀(PO₄)₄(CO₃)₂(OH)₄ (CO₃-HAP) (01-085-7370), calcium-deficient hydroxyapatite Ca_{8,86}(PO₄)₆(H₂O)₂ (dHAP) (01-082-1943), β -tricalcium phosphate (β -TCP) (01-070-2065), dicalcium phosphate dihydrate CaHPO₄·2H₂O (DCPD) (01-072-0713), α -tricalcium phosphate (01-070-0364), and calcium carbonate (01-072-1652). On the X-ray (Figure 1), calcium-deficient and carbonate-substituted hydroxyapatites are not marked in separate phases, due to the coincidence of the main peaks. In the course of quantitative phase analysis, the calculation was carried out based on the characteristic peaks at the interplane distance of 2.7309 and 1.9489 for dHAP, and of 2.8066 and 2.7782 for CO₃-HAP.

The presence of phases of the initial components is explained by the incompleteness of the reaction. Upon contact with water, dissolution reactions began to take place on the contact surface of the initial particles, in connection with which the water began to be saturated with OH[−], HPO₄^{2−}, Ca²⁺, and H₂PO₄[−] ions, and crystals of reaction products formed on the surface of the initial particles.

The amount of the initial phase of α -TCP decreased with increasing temperature. DCPD is an additional phase in the composition of ceramics; it is a product of the interaction of calcium carbonate and α -TCP with monocalcium phosphate monohydrate (MCPM). The presence of an impurity phase of β -TCP in the composition of ceramics was caused by the formation of about 8% of the polymorphic form of β -TCP during the solid-phase synthesis of α -TCP.

Identification of calcium carbonate by X-ray was impossible, since there were no characteristic peaks (i.e., not coinciding with the peaks of the present phases) in this system. When calculating the quantitative phase composition, calcium carbonate was not taken into account.

In accordance with the FTIR spectra, calcium carbonate was present in the composition of the chemically bonded ceramics based on α -TCP with a particle size of 6.12 microns in the initial consolidation periods at 60 °C (Figure 2).

The change in the peak intensity of the FTIR spectra of the ceramics, characteristic of calcium carbonate, confirms the course of the chemical reactions over 72 h.

The most intense and high-frequency band at 1435 cm^{−1} is not characteristic of the calcium carbonate spectrum, since it merges with the duplex characteristic of CO₃^{2−} carbonate-substituted hydroxyapatite ions. The intense bands at about 1409–1423 cm^{−1} and 1449–1474 cm^{−1} in the spectrum belong to the ν_3 mode of antisymmetric stretching, characteristic of CO₃^{2−}—ions in the A- (substitution of OH[−]—ions) and B-types (substitution of PO₄^{3−}—ions) of carbonate-substituted hydroxyapatite.

The bands at 712 and 875 cm^{−1} correspond to the deformation vibrations of calcium carbonate ions (CO₃^{2−}), and the band at 712 cm^{−1} can be considered characteristic, allowing us to judge the presence or absence of calcite in the composition. The band at 874 cm^{−1} coincides with the oscillations characteristic of HPO₄^{2−} ions. With increasing exposure time in a humid environment, the intensity of the peak at 712 cm^{−1} decreased, and it was not observed after 48 h. On the FTIR spectra of calcium carbonate, a peak at the band 1805 cm^{−1} was observed, which was also present during the initial hydration periods, but absent on the spectra after 24 h. Intense bands around 1409–1423 cm^{−1} and 1449–1474 cm^{−1} remained in

the absence of characteristic peaks of calcium carbonate, and the duplex was clearly visible, making it possible to assert that one phase was carbonate-substituted hydroxyapatite.

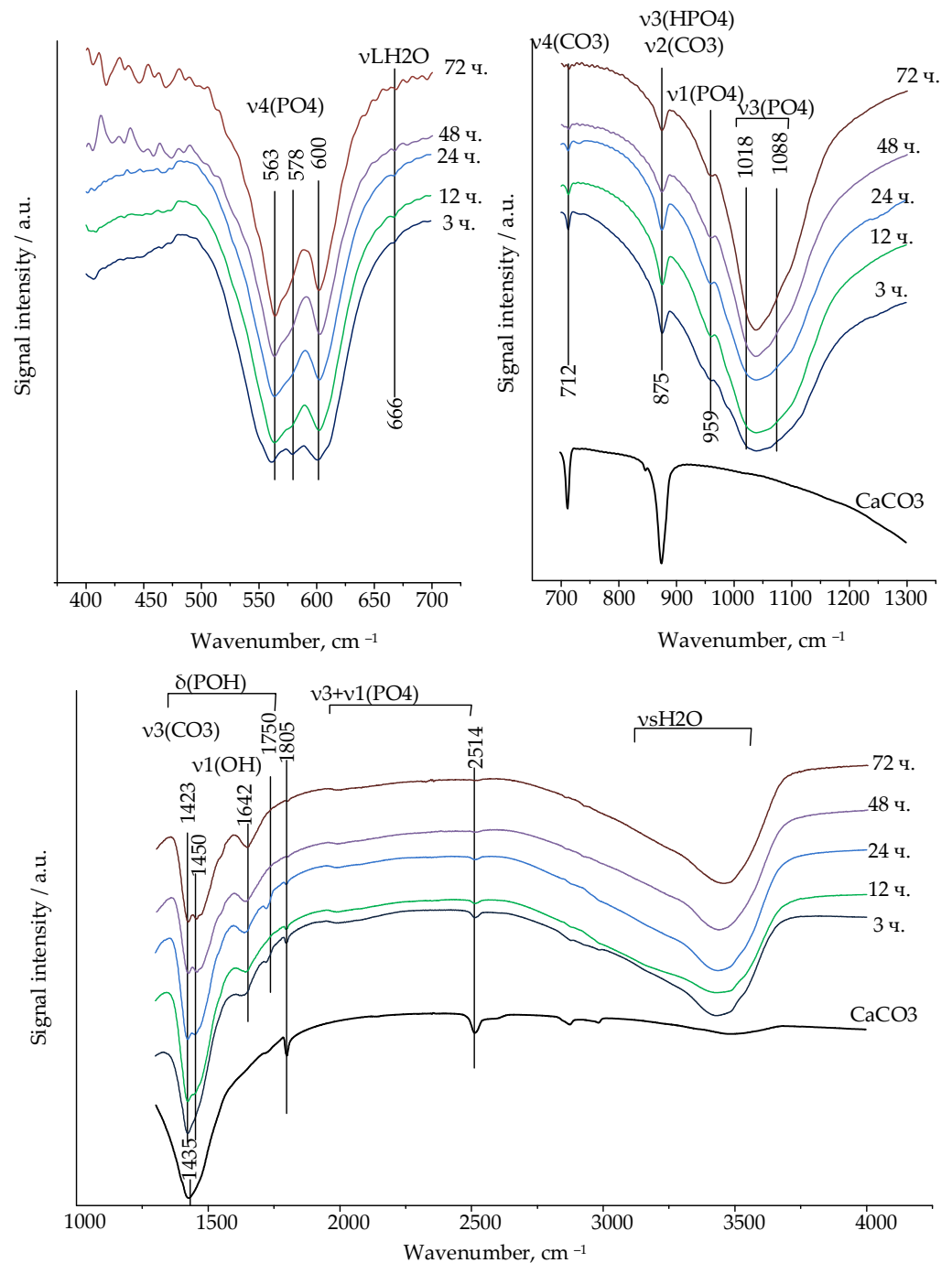


Figure 2. FTIR spectra of ceramics at different consolidation times, and FTIR spectra of calcium carbonate.

Fluctuations in the HPO_4^{2-} anion in the range of $1400\text{--}1750\text{ cm}^{-1}$ are characteristic, but due to the superposition of $\delta(\text{POH})$ oscillations on the fluctuations of $\nu_3(\text{CO}_2)$, we consider fluctuations in the range of $1600\text{--}1750\text{ cm}^{-1}$ to be the determining factor. Peaks at 1642 cm^{-1} are clearly defined on the spectrum, determining the ions of HPO_4^{2-} in the calcium-deficient hydroxyapatite.

Orthophosphoric tetrahedral ions in a hydroxyapatite-type structure are characterized by ν_4 bending (559–566, 571–578, 600–602 cm^{-1}), ν_1 symmetric stretching (960 cm^{-1}), and ν_3 antisymmetric stretching (1018–1050 and 1087–1090 cm^{-1}).

The kinetics of the formation of hydroxyapatites during the consolidation of ceramics at different temperatures and times, depending on the particle size of α -TCP, are shown in Figure 3.

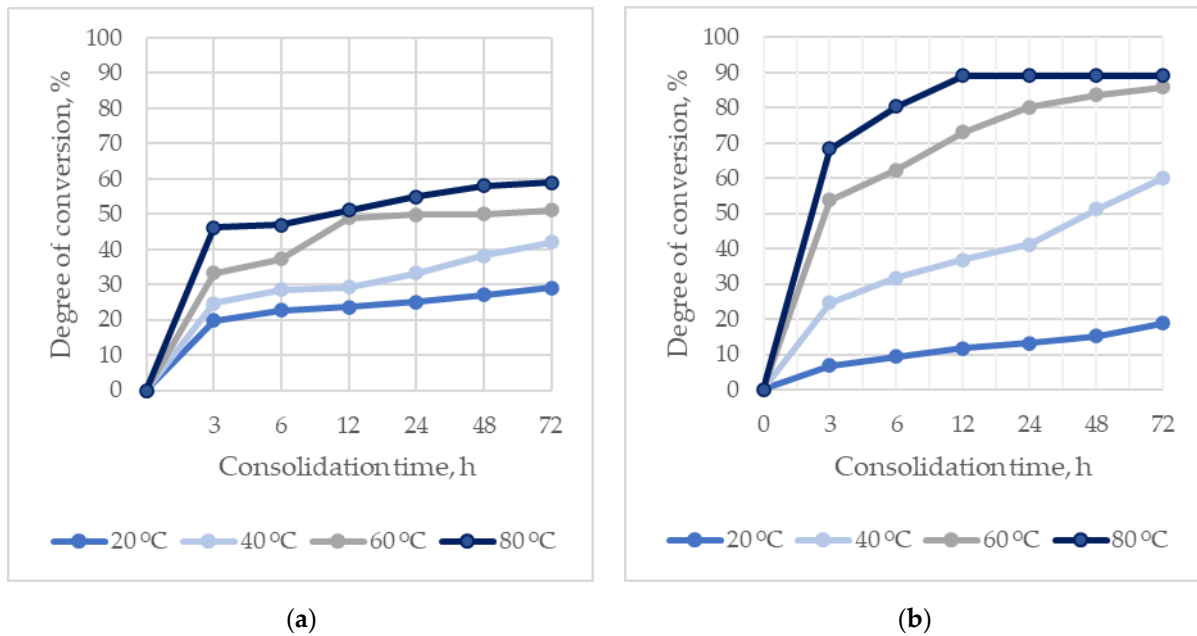


Figure 3. Kinetic curves of hydroxyapatite formation during consolidation of ceramics based on α -TCP with the following particle sizes: (a) D [3,4] 37.02 μm (α -TCP1); (b) D [3,4] 6.12 μm (α -TCP2).

The rate of formation of hydroxyapatites directly depends on the temperature, and increases with a decrease in the particle size of α -TCP.

The maximum degree of conversion of the initial components into hydroxyapatites is 89 wt.%, due to the presence of additional phases in the composition of the reaction products: DCPD and β -TCP. The amount of hydroxyapatites exceeds 80 wt.% at temperatures of 60–80 °C and a consolidation time of 24 h.

The low reaction rate in the case of using α -TCP1 (D [3,4] 37.02 μm) negatively affects the mechanical strength of the ceramics. The compressive strength of ceramics based on α -TCP1 during consolidation for 24 h at a temperature of 60 °C was 43.8 MPa, whereas for α -TCP2 (D [3,4] 6.12 μm) it was 68.88 MPa.

The results of scanning electron microscopy confirmed the formation of hydroxyapatite crystals on the surface of the initial particles, consolidating the matrix (Figure 4). At temperatures of 20 and 40 °C, after 72 h of ceramic consolidation, individual particles of the initial components were distinguishable, on which hydroxyapatite crystals were formed. Unreacted α -TCP was present in the microphotographs in the form of dense particles with hydroxyapatite crystals on the surface. At temperatures of 60 and 80 °C, the structure of the material was consolidated by the formed interaction products.

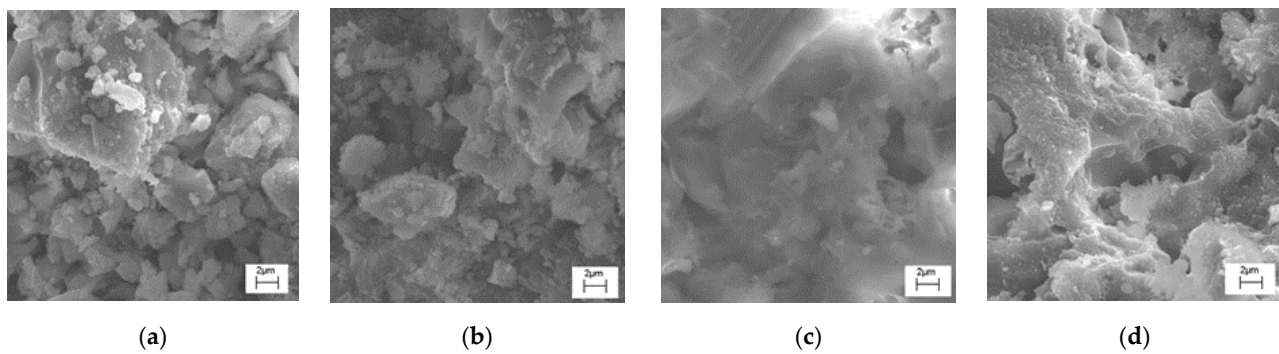


Figure 4. Micrographs of ceramics after 72 h of consolidation at temperatures of (a) 20 °C, (b) 40 °C, (c) 60 °C, and (d) 80 °C. Magnification $\times 6000$.

3.2. Properties of Ceramics

The macroporosity of ceramics is formed by extraction with organic solvents of polyethylene glycol (PEG) granules with a size of 100–600 microns, premixed with the initial dry mixture before forming via pre-pressing and consolidation. Chloroform was used as an extractant—not an aqueous medium—in order to avoid the extraction of vancomycin from the ceramics. It was found that the mass fraction of the residual polyethylene glycol was on average 0.9 wt.% of the total mass of samples, using the ^1H NMR method. After additional purification in the supercritical CO_2 medium, trace amounts of PEG were not detected, as confirmed by the results of the ^1H NMR study. The phase composition of porous ceramics was identical to that of dense ceramics, as confirmed by the X-ray data.

The porosity values exceeded the values of the introduced PEG due to the microporosity formed by the dissolution of $\text{Na}_2\text{HPO}_4 \cdot 12\text{H}_2\text{O}$ salt particles, the air involved in the matrix during its pressing, and the formation of CO_2 during the acid–base interaction of CaCO_3 with $\text{Ca}(\text{H}_2\text{PO}_4)_2 \cdot \text{H}_2\text{O}$. When PEG was introduced into the initial mixture, the porosity consisted of micro- and macroporosity formed due to the extraction of PEG granules from the matrix (Figure 5).

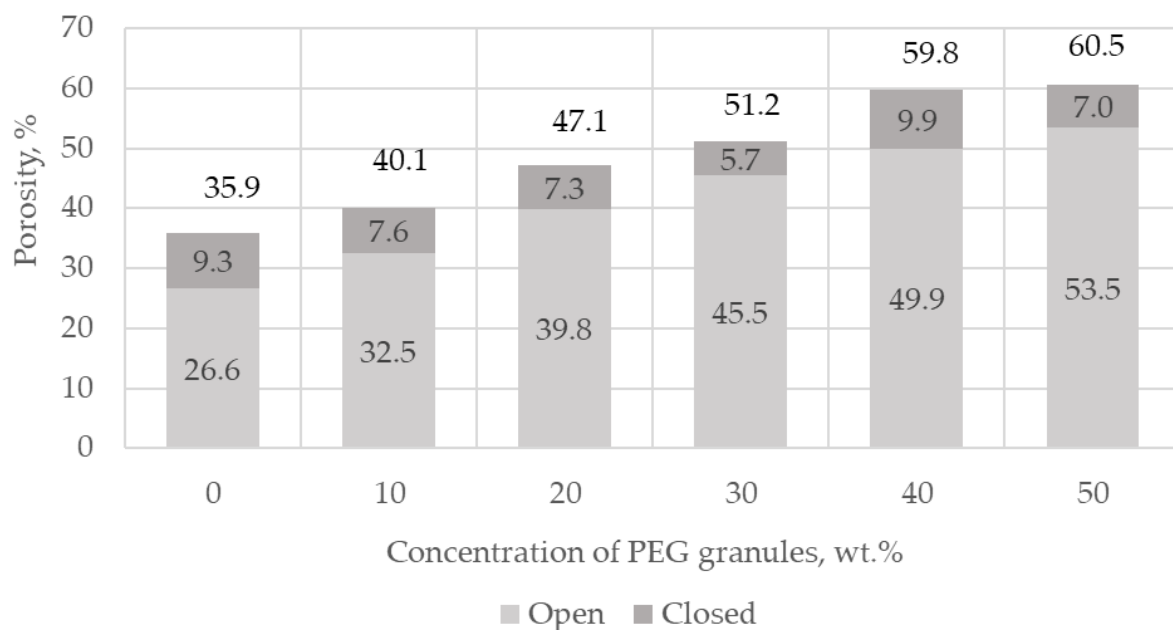


Figure 5. Porosity of ceramics.

According to micro-CT data, the distribution of PEG granules in the matrix was uniform, and the shape of the macropores differed from spherical, constituting an ellipsoid of rotation, due to the applied uniaxial load during matrix molding (Figure 6). The ratio of

the large axis of the ellipsoid to the small one was 1.5. We obtained the expected results on the distribution of macropores by size, based on the conservation of the volume of the PEC particles and the change from a spherical shape to an ellipsoid of rotation. In all samples, this was approximately equal to the distribution of PEG particles in size: 500–600 microns—19%, 400–500 microns—23%, 350–400—8%, 250–350—28%, 100–250—22%. The deviation from these values was insignificant; it decreased with increasing porosity, and was associated with the presence of compressed air.

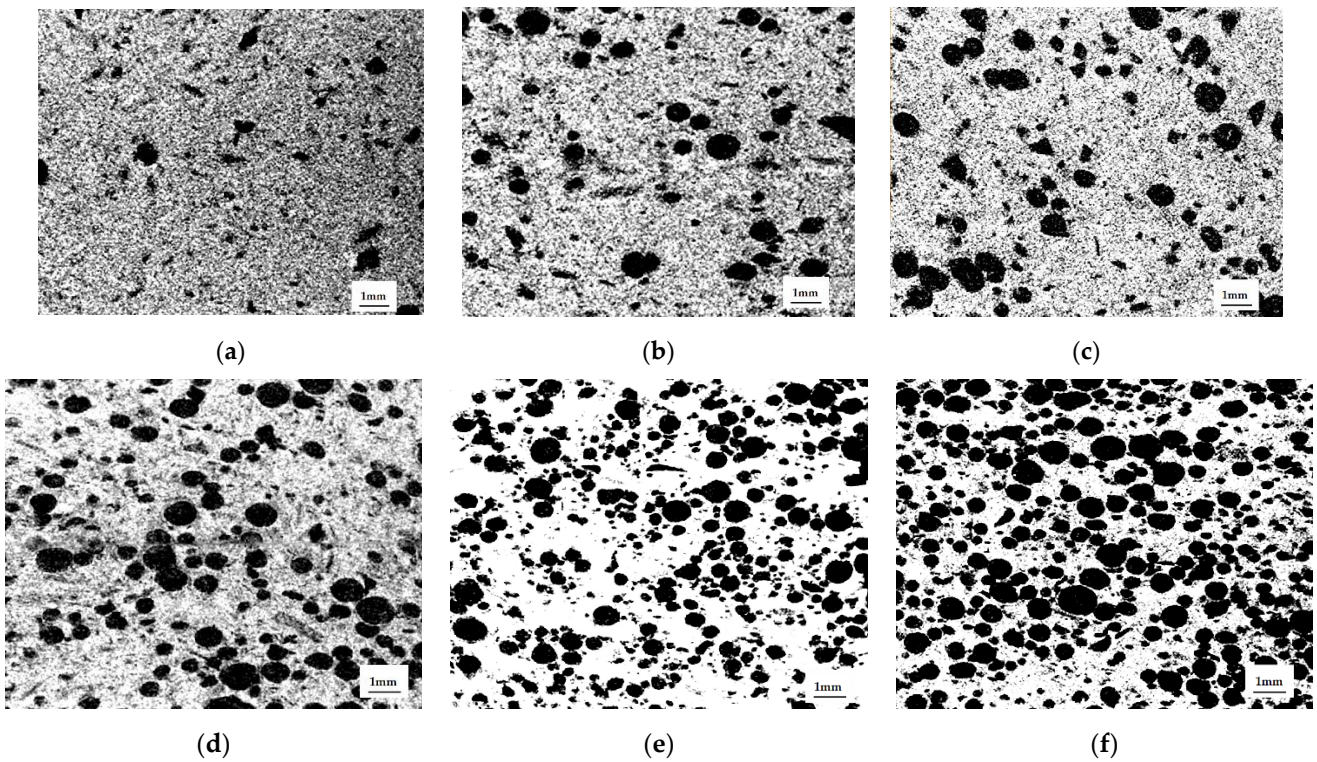


Figure 6. Micro-CT of ceramics after extraction of PEG granules in the following amounts: (a) 0%; (b) 10%; (c) 20%; (d) 30%; (e) 40%; (f) 50%.

The mechanical strength of chemically bonded ceramics is inversely proportional to the concentration of PEG granules (wt.%) (Figure 7). The change in the mechanical strength of ceramics is associated with a decrease in the number of contacts of the mineral component of the consolidated matrix.

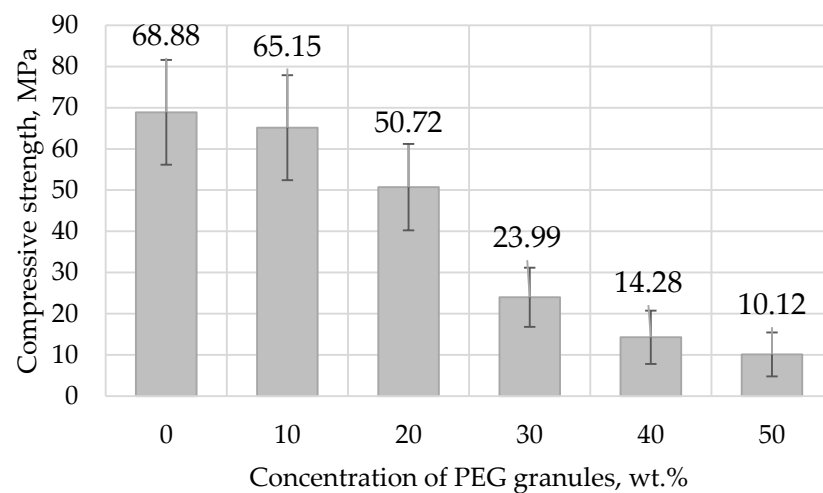


Figure 7. Mechanical strength of ceramics.

3.3. Incorporation of Vancomycin into Chemically Bonded Ceramics

We used vancomycin hydrochloride (hereafter referred to as vancomycin) in a freeze-dried form as an antibacterial substance. Vancomycin (gross formula $C_{66}H_{75}C_{12}N_9O_{24}$) is a glycopeptide containing a significant amount of halogenated and hydroxylated aromatic amino acids. Incorporation of antibacterial substances ensures prolongation of their yield at the implantation site compared to the rate of yield during product impregnation.

Vancomycin lyophilizate was injected at 150–300 mg/3 cm³ of ceramic matrix. In the process of hydration, a partial dissolution of vancomycin occurred, the solution of which impregnated the matrix. Simultaneously with vancomycin, $Na_2HPO_4 \cdot 12H_2O$ particles were dissolved, and phosphate ions were released into the solution, which caused the nucleation of hydroxyapatite in accordance with the concept of the “common ion effect” [29], and indirectly affected the solubility of α -TCP since, when saturated with Ca^{2+} and PO_4^{3-} ions, α -TCP does not dissolve until hydroxyapatite is precipitated from it. As soon as hydroxyapatite was formed, calcium and phosphate ions saturated the solution again, and more α -TCP could dissolve, accelerating the consolidation.

The $Na_2HPO_4 \cdot 12H_2O$ solution interacts with vancomycin, embedding phosphate ions into its structure. Absorption bands characteristic of $Na_2HPO_4 \cdot 12H_2O$ appeared on the IR spectrum of vancomycin after treatment with $Na_2HPO_4 \cdot 12H_2O$ solution, at 2466, 517, 511, 860, 957, and 991 cm⁻¹ (Figure 8).

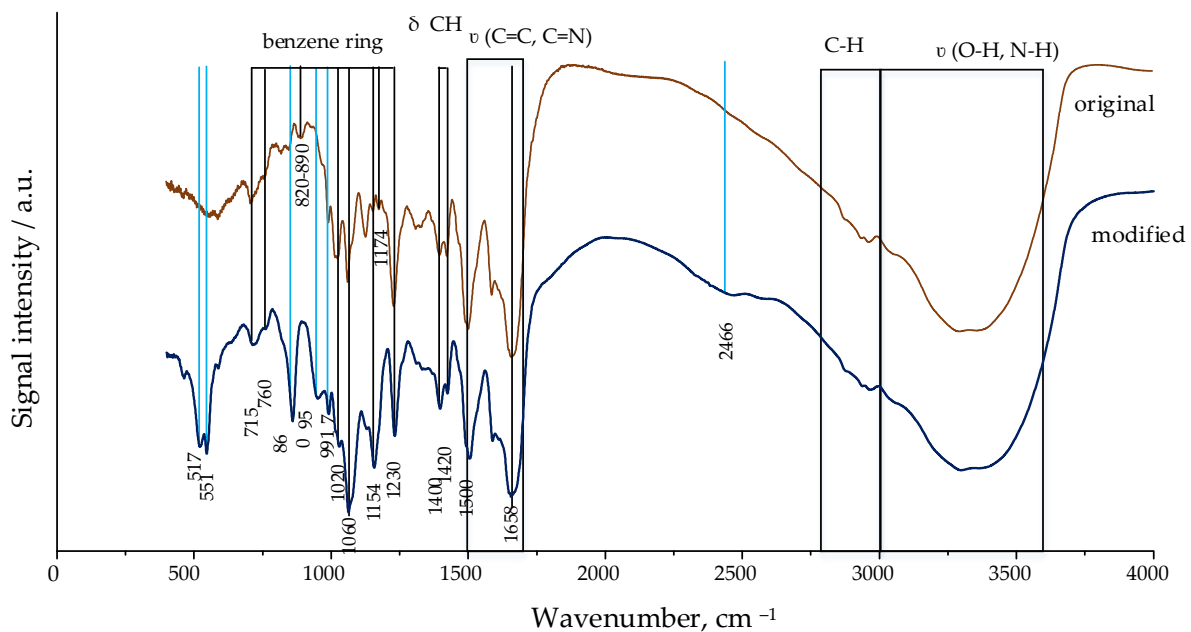


Figure 8. FTIR spectra of vancomycin: original, and after interaction with $Na_2HPO_4 \cdot 12H_2O$.

On the surface of the vancomycin particles, when exposed to sodium hydrophosphate salt, surges formed (Figure 9).

Vancomycin inside the matrix was located in the interstitial space in the form of flat crystal accretions, and was absorbed into the calcium phosphate matrix of the ceramics, as confirmed by the data of scanning electron microscopy and energy dispersion analysis (Figure 10).

According to the results of high-performance liquid chromatography obtained by measuring the concentration of the antibiotic in chloroform after using it to extract PEG granules from ceramics, the loss of vancomycin was less than 0.01%.

The dynamics of the output of vancomycin are shown in Figure 11. For 75 h, the proportion of the released antibiotic was from 23 wt.% to 57 wt.%, and depended on the amount of antibiotic and the porosity. The initial release in 5 h was from 10 wt.% to 39 wt.% of the total amount of the incorporated antibiotic, which occurred mainly due to diffusion. The exit speed

slowed down over time, but did not reach a plateau within 75 h. Vancomycin, dissolving inside the matrix in liquid, exited through interconnected pores. The greater the surface area (i.e., the greater the open porosity), the higher the rate of antibiotic release (Figure 12).

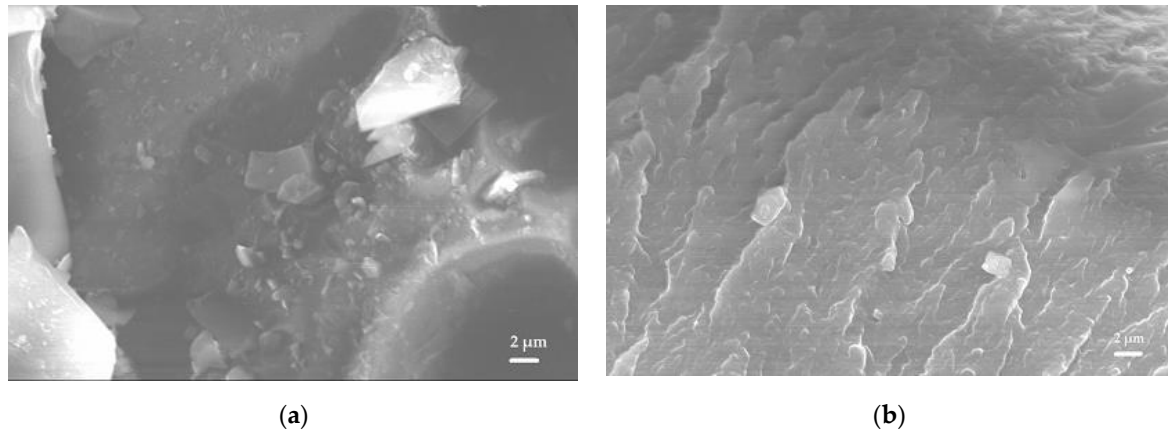
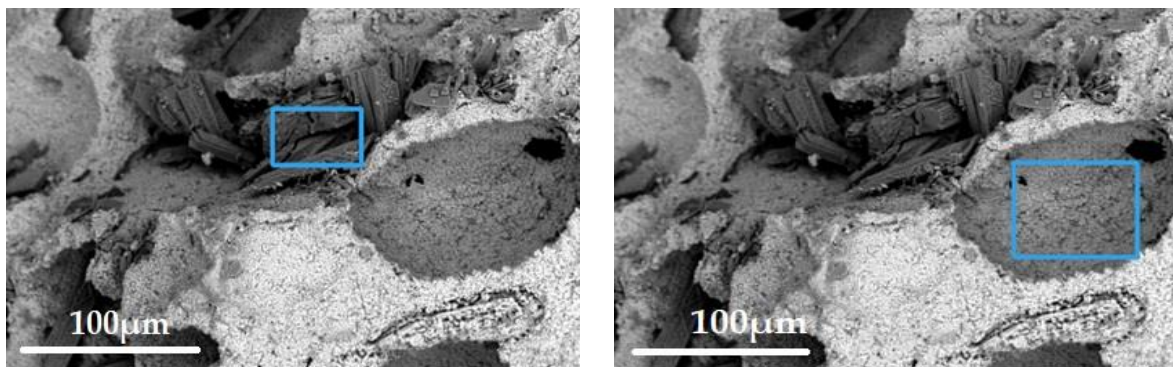


Figure 9. Micrographs of vancomycin: (a) initial; (b) after interaction with Na₂HPO₄·12H₂O.



Elemental Symbol	Atomic Conc.	Weight Conc.
C	55.22	46.73
N	21.89	21.61
O	18.72	21.11
P	0.69	1.51
Cl	2.41	6.03
Ca	1.07	3.02

Elemental Symbol	Atomic Conc.	Weight Conc.
C	15.60	9.00
O	57.89	44.50
Na	0.45	0.50
P	9.40	14.00
Cl	0.29	0.50
Ca	16.36	31.49

Figure 10. Microstructure of ceramics containing vancomycin, and results of EDX of the area bounded by a blue border.

Volumetric incorporation of vancomycin into the α -Ca₃(PO₄)₂/CaCO₃/Ca(H₂PO₄)₂·H₂O/Na₂HPO₄·12H₂O system retained its activity, as determined by measurements of the growth delay (inhibition) zones of bacterial cultures of *Staphylococcus aureus* (Gram-positive) (Table 2) and *Escherichia coli* (Gram-negative) (Table 3) after incubation for 31 days.

Ceramics containing 30% PEG granules in the initial mixture inhibited the growth of *S. aureus* bacteria for about 15 days at a vancomycin concentration of 150–200 mg in 3 cm³, and for 17 days at a concentration of 250–300 mg, while inhibiting *E. coli* for 16 days at a vancomycin concentration of 150–200 mg, and 22 days at a concentration of 250–300 mg, after which the effectiveness decreased. An increase in porosity due to an increase in the number of PEG granules increased the rate of antibiotic release. Similar to the positive

control, effective suppression of *S. aureus* for vancomycin concentrations of 250–300 mg was limited to 9 days, while suppression of *E. coli* was limited to 4 days.

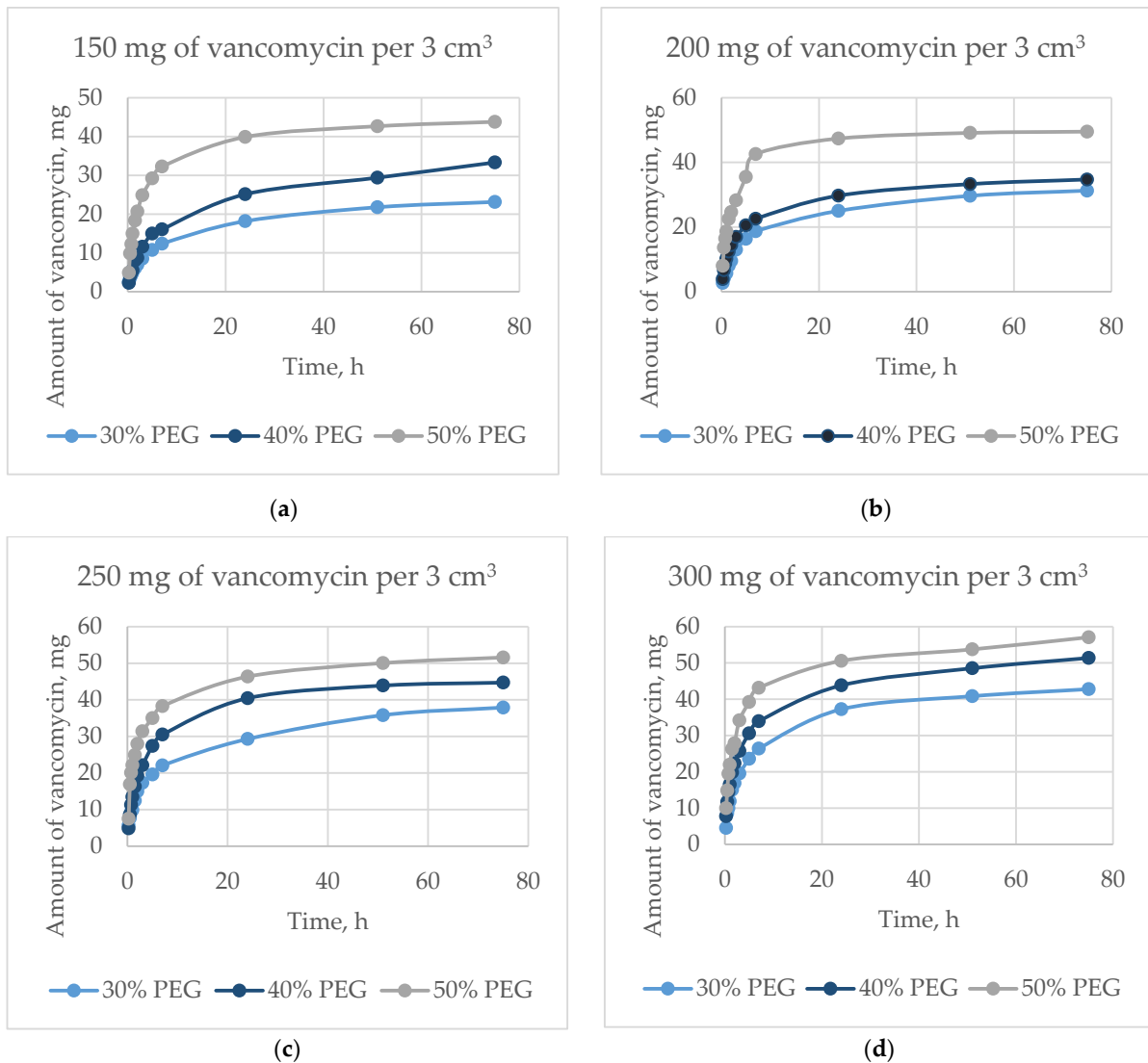


Figure 11. Dynamics of the release of vancomycin from the matrix at initial contents of (a) 150 mg, (b) 200 mg, (c) 250 mg, and (d) 300 mg.

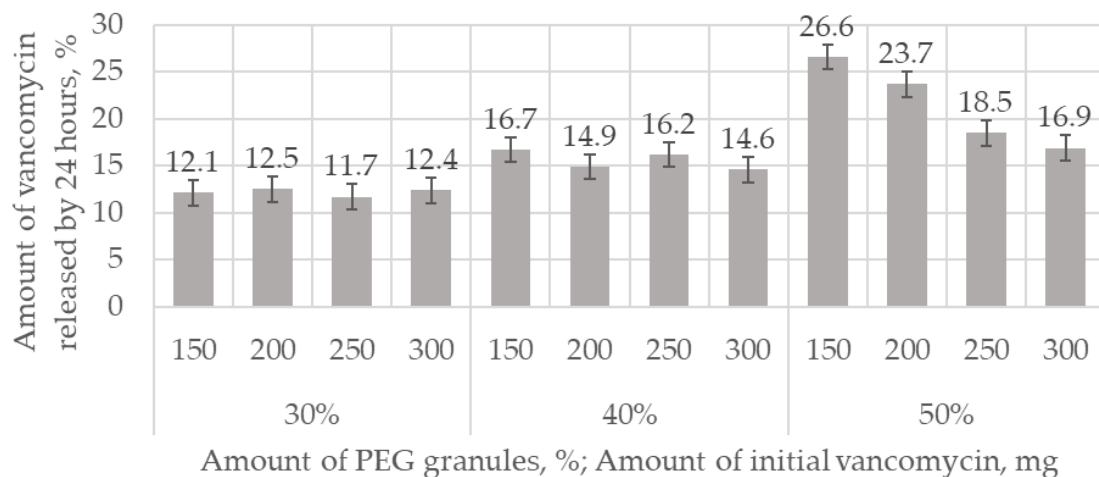


Figure 12. The amount of vancomycin released into the solution from the initial content by 24 h, wt.%.

Table 2. Diameters of growth retardation zones of bacterial cultures of *Staphylococcus aureus* with chemically bonded ceramics containing vancomycin, in comparison with negative and positive controls.

Amount of Vancomycin, mg	Time, h																															
	24	48	72	96	120	144	168	192	216	240	264	288	312	336	360	384	408	432	456	480	504	528	552	576	600	624	648	672	696	720	744	
Amount of PEG Granules in the Initial Mixture—30%																																
K+	16	16	16	16	16	16	16	16	16	16	16	16	16	16	16	16	16	16	16	16	16	16	16	16	16	16	16	16	16	16	16	16
K ₁	0	0	0	0	0	0	0	0	0	0	0	0	0	0	0	0	0	0	0	0	0	0	0	0	0	0	0	0	0	0	0	0
K ₂	0	0	0	0	0	0	0	0	0	0	0	0	0	0	0	0	0	0	0	0	0	0	0	0	0	0	0	0	0	0	0	0
150	18	17	15	14	13	14	14	14	13	12	12	12	11	11	11	10	9	9	9	8	7	7	6	0	0	0	0	0	0	0	0	0
200	22	18	17	16	16	17	16	16	15	14	13	13	13	12	11	10	10	9	9	8	8	7	7	6	0	0	0	0	0	0	0	0
250	21	19	17	16	16	16	16	16	16	15	14	14	14	14	12	11	11	10	10	10	9	9	8	7	7	6	0	0	0	0	0	0
300	20	18	19	16	18	18	18	17	16	15	15	14	14	14	14	12	12	11	11	10	10	10	9	9	8	7	6	0	0	0	0	0
Amount of PEG granules in the initial mixture—40%																																
K+	16	16	16	16	16	16	16	16	16	16	16	16	16	16	16	16	16	16	16	16	16	16	16	16	16	16	16	16	16	16	16	16
K ₁	0	0	0	0	0	0	0	0	0	0	0	0	0	0	0	0	0	0	0	0	0	0	0	0	0	0	0	0	0	0	0	0
K ₂	0	0	0	0	0	0	0	0	0	0	0	0	0	0	0	0	0	0	0	0	0	0	0	0	0	0	0	0	0	0	0	0
150	20	17	16	15	14	15	15	14	14	13	13	11	10	10	10	10	8	7	7	7	7	0	0	0	0	0	0	0	0	0	0	0
200	20	18	16	16	15	16	15	14	14	13	12	11	10	10	10	8	7	7	6	6	0	0	0	0	0	0	0	0	0	0	0	0
250	21	19	18	16	16	17	17	16	16	15	14	14	14	14	13	11	11	11	10	10	9	8	8	7	6	0	0	0	0	0	0	0
300	22	20	19	18	18	18	17	17	16	15	14	14	13	13	13	11	11	10	9	9	8	8	7	6	6	0	0	0	0	0	0	0
Amount of PEG granules in the initial mixture—50%																																
K+	16	16	16	16	16	16	16	16	16	16	16	16	16	16	16	16	16	16	16	16	16	16	16	16	16	16	16	16	16	16	16	16
K ₁	0	0	0	0	0	0	0	0	0	0	0	0	0	0	0	0	0	0	0	0	0	0	0	0	0	0	0	0	0	0	0	0
K ₂	0	0	0	0	0	0	0	0	0	0	0	0	0	0	0	0	0	0	0	0	0	0	0	0	0	0	0	0	0	0	0	0
150	21	18	17	16	13	16	16	14	14	12	11	11	10	9	9	8	7	6	0	0	0	0	0	0	0	0	0	0	0	0	0	0
200	21	19	18	16	14	15	14	14	14	13	13	12	10	9	9	7	7	6	6	0	0	0	0	0	0	0	0	0	0	0	0	0
250	21	20	18	17	15	15	15	15	15	14	13	12	11	11	8	8	8	7	7	6	6	0	0	0	0	0	0	0	0	0	0	0
300	22	21	19	18	16	16	16	16	16	15	14	13	13	13	12	9	9	8	8	7	6	6	0	0	0	0	0	0	0	0	0	0
«K ₁ »	—negative control (0.9% saline sodium chloride solution);																															
«K ₂ »	—sterile saline 0.9% sodium chloride solution after incubation with a test sample without vancomycin at 37 °C;																															
«K+»	—disc CAC—CAC30/10—ceftazidime 30 µg/ clavulanic acid 10 µg;																															
	—no growth delay zone or visible secondary growth																															

Table 3. Diameters of growth retardation zones of bacterial cultures of *Escherichia coli* with chemically bonded ceramics containing vancomycin, in comparison with negative and positive controls.

Amount of Vancomycin, mg	Time, h																											
	24	48	72	96	120	144	168	192	216	240	264	288	312	336	360	384	408	432	456	480	504	528	552	576	600	624	648	672
	Amount of PEG granules in the initial mixture—30%																											
K+	18	17	17	17	17	17	17	17	17	17	17	17	17	17	17	17	17	17	17	17	17	17	17	17	17	17	17	17
K ₁	0	0	0	0	0	0	0	0	0	0	0	0	0	0	0	0	0	0	0	0	0	0	0	0	0	0	0	0
K ₂	0	0	0	0	0	0	0	0	0	0	0	0	0	0	0	0	0	0	0	0	0	0	0	0	0	0	0	0
150	20	16	15	14	13	14	12	12	11	10	10	9	8	7	7	7	0	0	0	0	0	0	0	0	0	0	0	0
200	21	18	17	17	16	15	14	13	13	12	11	10	9	8	8	7	0	0	0	0	0	0	0	0	0	0	0	0
250	20	19	17	17	16	16	15	15	15	14	14	13	12	11	10	9	9	8	8	7	6	6	0	0	0	0	0	0
300	21	20	18	18	16	16	16	16	15	14	14	13	12	10	10	9	9	8	8	8	7	6	0	0	0	0	0	0
	Amount of PEG Granules in the Initial Mixture—40%																											
K+	17	16	17	17	17	17	17	17	17	17	17	17	17	17	17	17	17	17	17	17	17	17	17	17	17	17	17	17
K ₁	0	0	0	0	0	0	0	0	0	0	0	0	0	0	0	0	0	0	0	0	0	0	0	0	0	0	0	0
K ₂	0	0	0	0	0	0	0	0	0	0	0	0	0	0	0	0	0	0	0	0	0	0	0	0	0	0	0	0
150	20	17	16	15	14	15	13	13	12	12	11	10	7	7	7	7	0	0	0	0	0	0	0	0	0	0	0	0
200	20	18	16	16	15	14	12	11	10	10	8	8	6	6	6	0	0	0	0	0	0	0	0	0	0	0	0	0
250	21	19	18	16	16	16	15	15	14	14	14	13	12	12	10	9	9	8	7	0	0	0	0	0	0	0	0	0
300	22	20	19	18	16	16	16	14	14	13	12	11	11	10	9	8	7	6	0	0	0	0	0	0	0	0	0	0
	Amount of PEG Granules in the Initial Mixture—50%																											
K+	17	16	17	17	17	17	17	17	17	17	17	17	17	17	17	17	17	17	17	17	17	17	17	17	17	17	17	17
K ₁	0	0	0	0	0	0	0	0	0	0	0	0	0	0	0	0	0	0	0	0	0	0	0	0	0	0	0	0
K ₂	0	0	0	0	0	0	0	0	0	0	0	0	0	0	0	0	0	0	0	0	0	0	0	0	0	0	0	0
150	21	18	17	16	13	16	13	11	9	9	9	6	5	0	0	0	0	0	0	0	0	0	0	0	0	0	0	0
200	21	19	18	16	14	13	14	11	10	7	9	8	0	0	0	0	0	0	0	0	0	0	0	0	0	0	0	0
250	21	20	18	17	15	15	15	13	11	10	8	8	7	6	6	0	0	0	0	0	0	0	0	0	0	0	0	0
300	22	21	19	18	16	16	16	14	13	13	12	11	10	9	9	7	6	0	0	0	0	0	0	0	0	0	0	0
«K ₁ »	—negative control (0.9% saline sodium chloride solution);																											
«K ₂ »	—sterile saline 0.9% sodium chloride solution after incubation with a test sample without vancomycin at 37 °C;																											
«K+»	—disc CAC—CAC30/10—ceftazidime 30 µg/ clavulanic acid 10 µg;																											
	—no growth delay zone or visible secondary growth																											

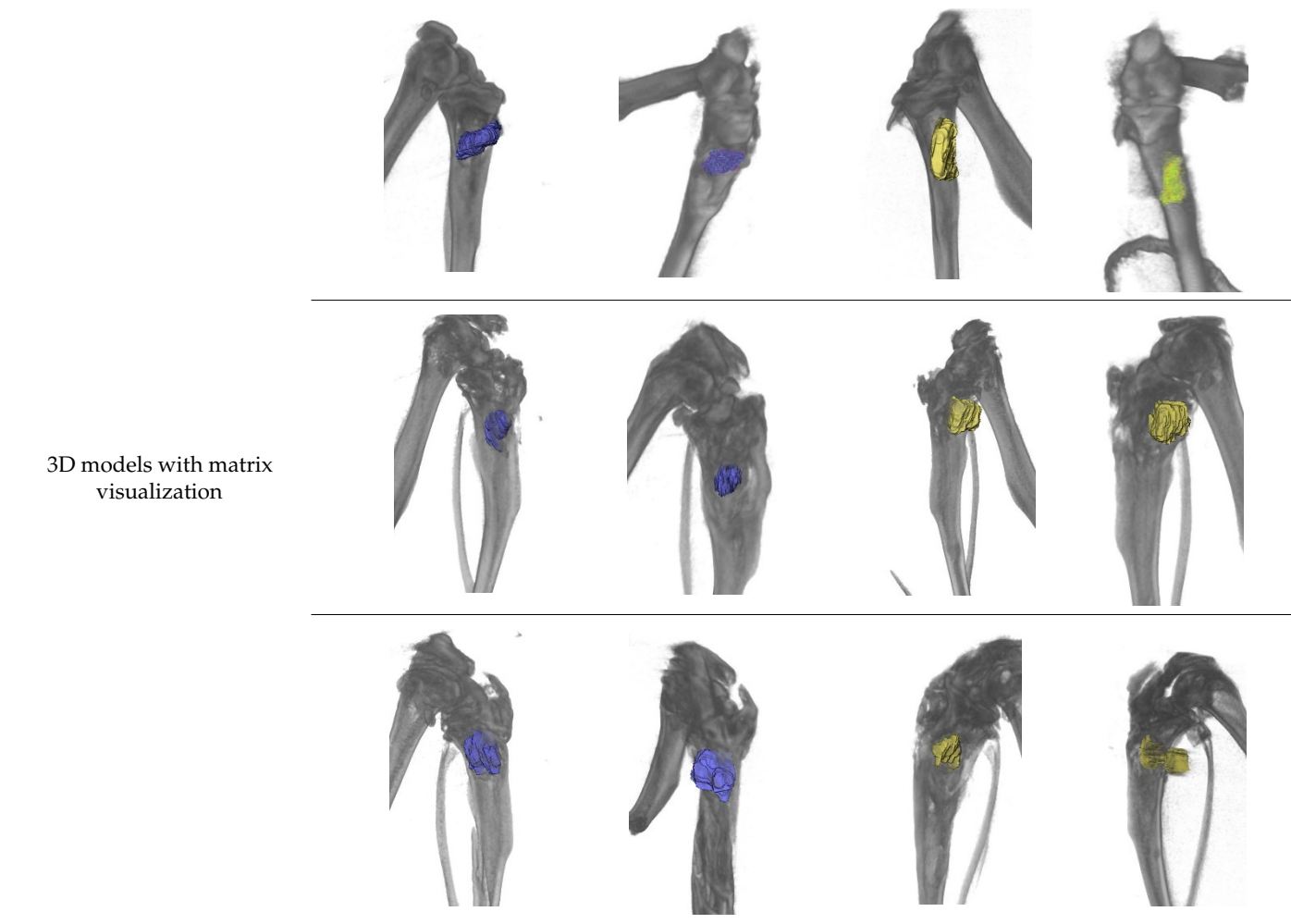
3.4. In Vivo Experiments

The antimicrobial activity of chemically bound ceramics was investigated via in vivo experiments on Wistar rats in a model of tibial bone perforation with pre-created purulent-septic inflammation, confirmed by morphological examination of biopsies taken before the implantation of matrices. To determine the antibacterial activity, the developed matrices were installed in bone perforations of critical size; a matrix without vancomycin (control) and a matrix with vancomycin (experiment) were installed in different limbs in one animal for comparison.

Three months after implantation, according to X-ray tomography, partial resorption of the matrix and the formation of new bone tissue occurred (Table 4).

Table 4. The volume of the implant and the 3D model of the tibia of a laboratory animal, created from CT results.

Implantation Period, Days.	Control		Experience	
	0	90	0	90
	39.72	39.10	32.35	23.56
Matrix volume, mm ³	21.14	17.00	35.55	23.40
	31.12	28.98	31.01	13.27

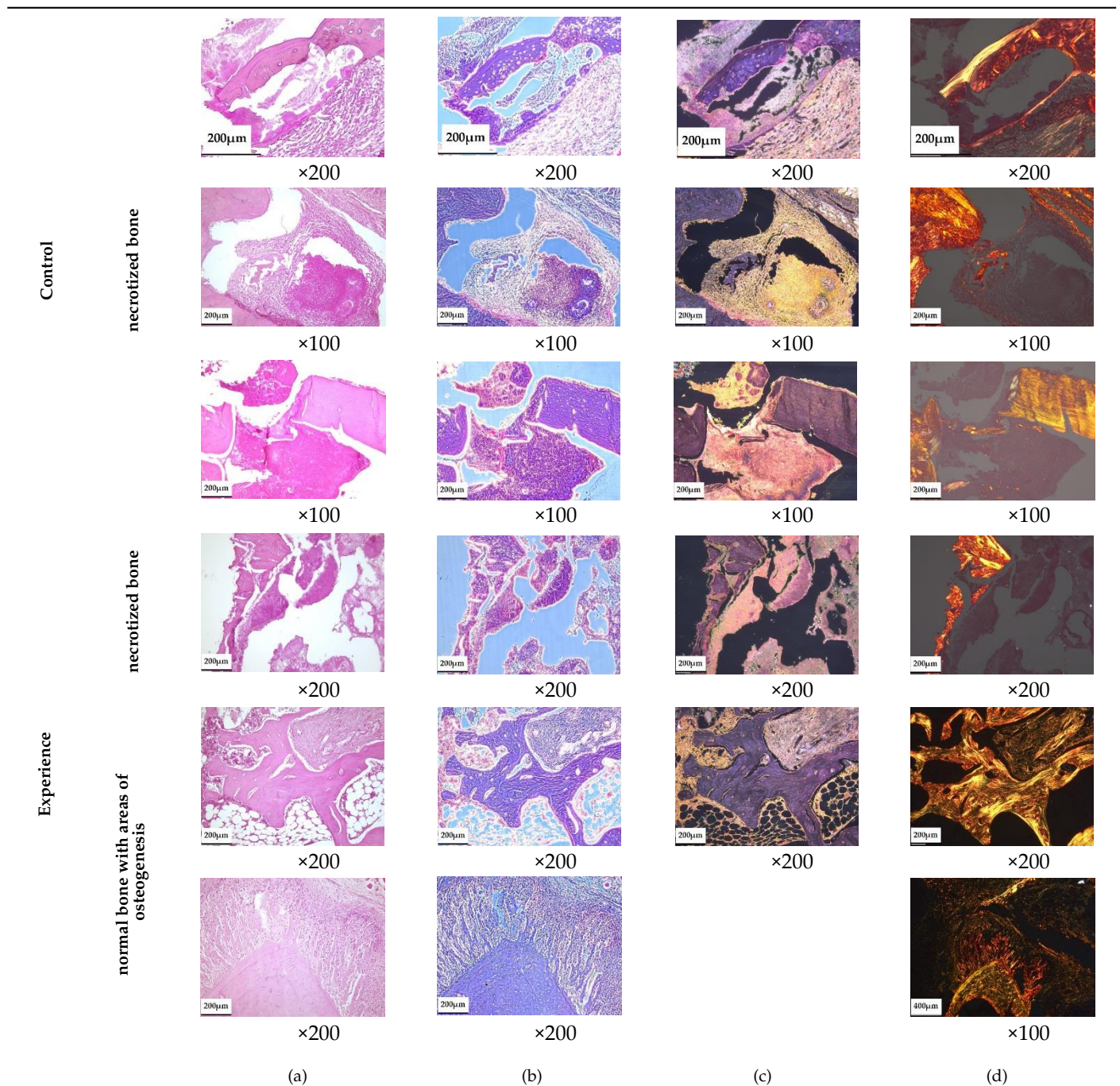


The average matrix resorption in three animals was 11% in the control group and 37% in the experimental group after three months of implantation.

According to the morphological study, 3 months after the implantation of chemically bonded ceramics, many large necrotized bone fragments without cellular elements and

with loosened and structurally damaged bone matrices were detected in all of the control samples (Table 5). Large areas of fibrous connective tissue with pronounced inflammatory infiltration (lymphocytes, macrophages, neutrophils) and in places with increased vascularization were observed in the affected area. Unlike normal bone, necrotized bone was unevenly stained with hematoxylin–eosin; with phase-contrast microscopy its thin, fibrous structure was not visible, and with picosirius staining and polarization microscopy it showed no anisotropy. Necrotic areas of bone are often surrounded by inflammatory infiltrate and fibrous connective tissue, with pronounced lymph–macrophage infiltration.

Table 5. Necrotized bone fragments: (a) Standard light microscopy; staining with hematoxylin–eosin. (b) Phase-contrast microscopy; staining with hematoxylin–eosin. (c) Dark-field microscopy; staining with hematoxylin–eosin. (d) Polarization microscopy; coloring with picosirius red.



Treatment of developed osteomyelitis with chemically bound ceramics containing vancomycin gave positive results; most of the bone tissue had a normal structure with areas of osteogenesis, and only small areas of bone underwent necrosis, although pronounced inflammatory infiltration persisted in the samples.

4. Discussion

The technology of chemically bonded ceramics combines the advantages of cement and ceramic technologies, and can be used to produce osteoplastic materials. Consolidation of matrices without heat treatment of the formed product enables the incorporation of functional substances such as antimicrobials, and high macroporosity in combination with strength characteristics comparable to those of calcium phosphate cements makes chemically bonded ceramics good osteoconductors. This not only allows the inflammatory process to be stopped at the same time, but also enables the closing of the bone defect.

The main component of chemically bonded ceramics is α -TCP, which is hydrolyzed to dHAP in aqueous media. Calcium carbonate was used to produce carbonate hydroxyapatite as the target phase. When mixed with α -TCP, it participates in the hydrolysis process, contributing to the incorporation of CO_3^{2-} ions into the crystal lattice [30]. $\text{Ca}(\text{H}_2\text{PO}_4)_2 \cdot \text{H}_2\text{O}$ and $\text{Na}_2\text{HPO}_4 \cdot 12\text{H}_2\text{O}$ reduce the Ca/P ratio. When replacing PO_4^{3-} with CO_3^{2-} or HPO_4^{2-} , a deficit of negative charge is formed, which is compensated for by a deficiency in calcium and the replacement of Ca^{2+} —ions with Na^+ .

The total Ca/P ratio of the initial components was 1.51, and the Ca/(P/C) was 1.33. This is significantly less than the Ca/P of stoichiometric hydroxyapatite (1.67). A decrease in the ratios leads to a deficiency in calcium, and the presence of carbonate ions leads to their incorporation into the crystal lattice of the resulting hydroxyapatite. As expected, the multiphase ceramics obtained in the process of low-temperature synthesis contained calcium-deficient and carbonate-substituted hydroxyapatite as the main phase, bringing the composition of the ceramic material as close as possible to the composition of bone tissue. The presence of non-target phases in the final composition—each of which has a higher solubility than the apatite phases—increases the resorption rate of the ceramics [31]. Macroporosity also contributes to this, increasing the area on top. The macroporosity obtained by extraction of PEG granules has a predetermined pore size distribution, and can be regulated by the size distribution of PEG particles, promote vascularization, and enable blood access to the contact surfaces of the matrix through the emerging network of blood capillaries, angiogenesis, and osseointegration.

Due to the introduction of antibiotic lyophilizate into the powder mixture before forming, the consolidation process cannot be carried out in an aqueous medium, or else the concentration of the antibiotic cannot be stored. Vancomycin has a high solubility in water, and diffuses through the pores during the formation of crystallohydrates in water. We used wet-air conditions when consolidating ceramics to solve this problem. This can negatively affect the completeness of the reaction and the properties of the ceramics.

The solution to the problem of the completeness of the reaction with the formation of final products and the consolidation of ceramics is possible by increasing the temperature of consolidation and shifting the granulometric composition towards smaller values. Faster dissolution of small particles promotes supersaturation and formation of crystalline nuclei.

In general, the results obtained showed that the particle size is a key factor that significantly changes the final properties of chemically bonded ceramics, and that particularly affects the reaction kinetics and physical and mechanical characteristics. Pre-pressing brings particles closer together, contributing to consolidation during chemical reactions, the speed of which depends—among other things—on temperature. An increase in temperature increases the solubility of the initial components and the rate of structure formation.

When choosing the consolidation temperature, it is necessary, on the one hand, to maintain the activity of the incorporated substances, and on the other hand, to maximize the completeness of the reactions. According to our results, a consolidation temperature of 60 °C leads to the production of ceramics based on the target hydroxyapatite phases,

while maintaining the activity of the vancomycin glycopeptide. Our microbiological study confirmed the preservation of the activity of the antibiotic when incorporated into the calcium phosphate matrix. This is due to the use of low-temperature technology, along with the absence of interaction with the initial components of the ceramics, except for the incorporation of phosphate ions into the structure of vancomycin, which does not affect the activity.

Calcium phosphate cements have been repeatedly investigated and used in a variety of drug delivery systems. Stallmann et al. [17] found that the rate of gentamicin release from calcium phosphate cements was more prolonged than that from impregnated calcium phosphate granules, due to the technology incorporated, i.e., the mixing procedure gave a more uniform distribution of the drug than the adsorption of the drug on an uneven porous surface. The dynamics of antibiotic yield depend on the composition and porosity of the calcium phosphate cement which, according to data from the literature, is 17–78% after 7 days [17,21], with a prolongation of more than 8 weeks in according to [32] when maintaining the level of vancomycin above the minimum suppressive concentration > 4 g/mL, and 17 days according to [17].

Chemically bonded ceramics, such as cements, gradually release vancomycin, prolonging its yield by up to 31 days. The profile of the release of vancomycin shows a curve with a large initial release followed by a slow release, fully confirming the authors' research [18,33,34]. The burst of release in the initial time period reflects the easy diffusion of the antibiotic from the surface layer. After this period of time, the diffusion of vancomycin from the inner surface of the matrix is somewhat difficult, which slows down its release and, thus, prolongs the output.

An increase in the surface area of the matrices (e.g., an increase in porosity) leads to an increase in the rate of release of vancomycin. The proportion of the antibiotic released into the solution from the initial amount is the same after 24 h for matrices whose porosity is formed by extraction of 30 and 40 wt.% PEG granules. The proportion of vancomycin derived from matrices formed by extraction of 50 wt.% PEG granules is inversely proportional to the initial concentration of vancomycin. This is due to a higher rate of vancomycin release in the initial period, along with the loss of antibacterial activity of matrices with high porosity in a shorter period.

It is difficult to extrapolate the results of our *in vitro* study to clinical concentrations in bones and surrounding tissues. The experiment did not take into account physiological parameters (e.g., the presence of blood flow, the pH of the medium, and other parameters that are difficult to transfer to *in vitro*); however, the same conditions were strictly observed for all samples for the purpose of comparative analysis among themselves and with positive controls during microbiological examination.

Uchida K. et al. [34] found that the amount of vancomycin released *in vivo* was about half of what was released *in vitro*, which may have been due to the smaller volume of fluid around the material *in vivo* compared to *in vitro*. The release of vancomycin *in vivo* can continue after day 56 at a concentration exceeding the MIC of 1.56 micrograms per day. Based on the research of Uchida K. et al., it can be assumed that the developed chemically bonded ceramics can significantly prolong the local yield of antibiotics.

Primary animal studies have confirmed the effectiveness of the incorporation of the antibiotic into chemically bonded calcium phosphate ceramics, since the treatment of the developed purulent inflammatory process caused by *S. aureus* reduced the amount of affected bone in the implantation zone. These studies are not statistically confirmed, but they give an idea of the potential therapeutic possibilities of chemically bonded ceramics containing antibacterial substances.

5. Conclusions

Chemically bonded microporous ceramics with the incorporated glycopeptide vancomycin have an effective profile of prolonged release, and can allow antibacterial therapy to be carried out locally, at the site of implantation.

Author Contributions: Conceptualization, Y.L.; methodology, Y.L., D.L., D.K., N.G. and S.S.; investigation, Y.L., Y.P., L.P., A.S., L.B.-A., N.S., O.T. and D.S.; writing—original draft preparation, Y.L.; writing—review and editing, Y.L.; visualization, Y.L., A.K., N.S. and L.B.-A.; supervision, Y.L.; project administration, Y.L. All authors have read and agreed to the published version of the manuscript.

Funding: This research received no external funding.

Institutional Review Board Statement: The protocol of the animal study was approved by the Local Ethical Committee for Medical and Biological Ethics of the N.N. Priorov National Medical Research Center for Traumatology and Orthopedics of the Ministry of Health of the Russian Federation (protocol code 004, approval date 5 May 2021).

Informed Consent Statement: Not applicable.

Data Availability Statement: Not applicable.

Conflicts of Interest: The authors declare no conflict of interest. The funders had no role in the design of the study; in the collection, analyses, or interpretation of data; in the writing of the manuscript; or in the decision to publish the results.

References

1. Pincher, B.; Fenton, C.; Jeyapalan, R.; Barlow, G.; Sharma, H.K. A systematic review of the single-stage treatment of chronic osteomyelitis. *J. Orthop. Surg. Res.* **2019**, *14*, 1–8. [[CrossRef](#)] [[PubMed](#)]
2. Masters, E.A.; Trombetta, R.P.; de Mesy Bentley, K.L.; Boyce, B.F.; Gill, A.L.; Gill, S.R.; Nishitani, K.; Ishikawa, M.; Morita, Y.; Ito, H.; et al. Evolving concepts in bone infection: Redefining “biofilm”, “acute vs. chronic osteomyelitis”, “the immune proteome” and “local antibiotic therapy”. *Bone Res.* **2019**, *7*, 2. [[CrossRef](#)] [[PubMed](#)]
3. Walter, G.; Kemmerer, M.; Kappler, C.; Hoffmann, R. Treatment Algorithms for Chronic Osteomyelitis. *Dtsch. Ärzteblatt Int.* **2012**, *109*, 257–266. [[CrossRef](#)] [[PubMed](#)]
4. Kavanagh, N.; Ryan, E.J.; Widaa, A.; Sexton, G.; Fennell, J.; O'Rourke, S.; Cahill, K.C.; Kearney, C.J.; O'Brien, F.J.; Kerrigan, S.W. Staphylococcal Osteomyelitis: Disease Progression, Treatment Challenges, and Future Directions. *Clin. Microbiol. Rev.* **2018**, *31*, e00084-17. [[CrossRef](#)] [[PubMed](#)]
5. Fraimow, H.S. Systemic Antimicrobial Therapy in Osteomyelitis. *Semin. Plast. Surg.* **2009**, *23*, 90–99. [[CrossRef](#)]
6. Sheehy, S.; Atkins, B.; Bejon, P.; Byren, I.; Wylie, D.; Athanasou, N.; Berendt, A.; McNally, M. The microbiology of chronic osteomyelitis: Prevalence of resistance to common empirical anti-microbial regimens. *J. Infect.* **2010**, *60*, 338–343. [[CrossRef](#)]
7. Mahmoudian, M.; Ganji, F. Vancomycin-loaded HPMC microparticles embedded within injectable thermosensitive chitosan hydrogels. *Prog. Biomater.* **2017**, *6*, 49–56. [[CrossRef](#)]
8. Nandi, S.K.; Bandyopadhyay, S.; Das, P.; Samanta, I.; Mukherjee, P.; Roy, S.; Kundu, B. Understanding osteomyelitis and its treatment through local drug delivery system. *Biotechnol. Adv.* **2016**, *34*, 1305–1317. [[CrossRef](#)]
9. Urish, K.L.; Cassat, J.E. Staphylococcus aureus Osteomyelitis: Bone, Bugs, and Surgery. *Infect. Immun.* **2020**, *88*, 1–43. [[CrossRef](#)]
10. Shi, M.; Zhang, P.; Zhao, Q.; Shen, K.; Qiu, Y.; Xiao, Y.; Yuan, Q.; Zhang, Y. Dual functional monocytes modulate bactericidal and anti-inflammation process for severe osteomyelitis treatment. *Small* **2020**, *16*, e1905185. [[CrossRef](#)] [[PubMed](#)]
11. Rowley, W.R.; Bezold, C.; Arikan, Y.; Byrne, E.; Krohe, S. Diabetes 2030: Insights from Yesterday, Today, and Future Trends. *Popul. Health Manag.* **2017**, *20*, 6–12. [[CrossRef](#)]
12. Wassif, R.K.; Elkayal, M.; Shamma, R.N.; Elkheshen, S.A. Recent advances in the local antibiotics delivery systems for management of osteomyelitis. *Drug Deliv.* **2021**, *28*, 2392–2414. [[CrossRef](#)]
13. Boles, L.R.; Awais, R.; Beenken, K.E.; Smeltzer, M.; Haggard, W.O.; Jessica, A.J. Local Delivery of Amikacin and Vancomycin from Chitosan Sponges Prevent Polymicrobial Implant-Associated Biofilm. *Mil. Med.* **2018**, *183* (Suppl. S1), 459–465. [[CrossRef](#)] [[PubMed](#)]
14. Van Vugt, T.A.G.; Heidotting, J.; Arts, J.J.; Ploegmakers, J.J.W.; Jutte, P.C.; Geurts, J.A.P. Mid-term clinical results of chronic cavitory long bone osteomyelitis treatment using S53P4 bioactive glass: A multi-center study. *J. Bone Jt. Infect.* **2021**, *6*, 413–421. [[CrossRef](#)] [[PubMed](#)]
15. Tao, F.; Ma, S.; Tao, H.; Jin, L.; Luo, Y.; Zheng, J.; Xiang, W.; Deng, H. Chitosan-based drug delivery systems: From synthesis strategy to osteomyelitis treatment—A review. *Carbohydr. Polym.* **2020**, *251*, 117063. [[CrossRef](#)] [[PubMed](#)]
16. Padrão, T.; Coelho, C.C.; Costa, P.; Alegrete, N.; Monteiro, F.J.; Sousa, S.R. Combining local antibiotic delivery with heparinized nanohydroxyapatite/collagen bone substitute: A novel strategy for osteomyelitis treatment. *Mater. Sci. Eng. C* **2020**, *119*, 111329. [[CrossRef](#)] [[PubMed](#)]
17. Anugraha, A.; Hughes, L.D.; Pillai, A. A novel technique for fabricating antibiotic-coated intramedullary nails using an antibiotic-loaded calcium sulphate hydroxyapatite bio-composite, Cerament-V. *J. Surg. Case Rep.* **2019**, *11*, rjz327. [[CrossRef](#)] [[PubMed](#)]
18. Young, A.M.; Ng, P.Y.U.J.; Gbureck, U.; Nazhat, S.H.N.; Barralet, J.E.; Hofmann, M.P. Characterization of chlorhexidine-releasing, fast-setting, brushite bone cements. *Acta Biomater.* **2008**, *4*, 1081–1088. [[CrossRef](#)] [[PubMed](#)]

19. Stallmann, H.P.; Faber, C.; Bronckers, A.L.J.J.; Amerongen, A.V.N.; Wuisman, P.I.J.M. In vitro gentamicin release from commercially available calcium-phosphate bone substitutes influence of carrier type on duration of the release profile. *BMC Musculoskelet. Disord.* **2006**, *7*, 7–18. [[CrossRef](#)] [[PubMed](#)]
20. Mukai, M.; Uchida, K.; Sugo, K.; Nakasu, M.; Nakajima, T.; Takata, K.; Takaso, M.; Urabe, K. Long-term antibacterial activity of vancomycin from calcium phosphate cement in vivo. *Bio-Medical Mater. Eng.* **2022**, *33*, 41–50. [[CrossRef](#)]
21. van de Belt, H.; Neut, D.; Uges, D.; Schenk, W.; van Horn, J.R.; van der Mei, H.C.; Busscher, H.J. Surface roughness, porosity and wettability of gentamicin-loaded bone cements and their antibiotic release. *Biomaterials* **2000**, *21*, 1981–1987. [[CrossRef](#)]
22. Sarigol-Calamak, E.; Hascicek, C. Tissue Scaffolds as a Local Drug Delivery System for Bone Regeneration. *Cut.-Edge Enabling Technol. Regen. Med.* **2018**, *1078*, 475–493. [[CrossRef](#)]
23. Takagi, S.; Chow, L.C. Formation of macropores in calcium phosphate cement implants. *J. Mater. Sci. Mater. Med.* **2001**, *12*, 135–139. [[CrossRef](#)] [[PubMed](#)]
24. Yin, Y.; Ye, F.; Yao, K.; Cui, J.; Song, X. Gelatin manipulation of latent macropores formulation in brushite cement. *J. Mater. Sci. Mater. Med.* **2003**, *14*, 255–261.
25. Silva, T.S.N.; Primo, B.T.; Silva, A.N., Jr.; Machado, D.C.; Viezzer, C.; Santos, A.L. Use of calcium phosphate cement scaffolds for bone tissue engineering: In vitro study. *Acta Cir. Bras.* **2011**, *26*, 7–11. [[CrossRef](#)]
26. Chow, L.C.; Takagi, S. Self-Setting Calcium Phosphate Cements and Methods for Preparing and Using Them. U.S. Patent No. 5,525,148, 11 June 1996.
27. Filippov, Y.Y.; Larionov, D.S.; Putlyaev, V.I.; Sokolov, A.V.; Koval’Kov, V.K.; Agakhi, K.A.; Selezneva, I.I.; Nikonova, Y.A. Reaction-Associated Resorbable Phosphate Materials: Production and Testing in Vitro. *Glas. Ceram.* **2013**, *70*, 306–310. [[CrossRef](#)]
28. Constantz, B.R.; Fulmer, M.T.; Barr, B.M. Prepared Calcium Phosphate Composition and Method. U.S. Patent No. 5,820,632, 13 October 1998.
29. Fernández, E.; Boltong, M.; Ginebra, M.-P.; Bermúdez, O.; Driessens, F.; Planell, J. Common ion effect on some calcium phosphate cements. *Clin. Mater.* **1994**, *16*, 99–103. [[CrossRef](#)]
30. Ginebra, M.-P.; Fernández, E.; Driessens, F.C.M.; Planell, J.A. Modeling of the Hydrolysis of α -Tricalcium Phosphate. *J. Am. Ceram. Soc.* **2004**, *82*, 2808–2812. [[CrossRef](#)]
31. Dorozhkin, S.V. Nanodimensional and nanocrystalline calcium orthophosphates. *Am. J. Biomed. Eng.* **2012**, *2*, 48–97. [[CrossRef](#)]
32. Chen, G.; Liu, B.; Liu, H.; Zhang, H.; Yang, K.; Wang, Q.; Ding, J.; Chang, F. Calcium Phosphate Cement loaded with 10% vancomycin delivering high early and late local antibiotic concentration in vitro. *Orthop. Traumatol. Surg. Res.* **2018**, *104*, 1271–1275. [[CrossRef](#)]
33. Qiu, G.; Huang, M.; Liu, J.; Wang, P.; Schneider, A.; Ren, K.; Oates, T.W.; Weir, M.D.; Xu, H.H.K.; Zhao, L. Antibacterial calcium phosphate cement with human periodontal ligament stem cell-microbeads to enhance bone regeneration and combat infection. *J. Tissue Eng. Regen. Med.* **2021**, *15*, 232–243. [[CrossRef](#)] [[PubMed](#)]
34. Uchida, K.; Sugo, K.; Nakajima, T.; Nakawaki, M.; Takano, S.; Nagura, N.; Takaso, M.; Urabe, K. In Vivo Release of Vancomycin from Calcium Phosphate Cement. *BioMed Res. Int.* **2018**, *2018*, 1–6. [[CrossRef](#)] [[PubMed](#)]